Analysing the Effect of Asymmetry on the Performance of Atomic Ensemble Based Repeater Protocols

Hana Jirovská

Delft University of Technology

27 June 2021

QuTech

Supervisor: David Maier
Responsible Professor: Prof. Dr. Stephanie Wehner
Examiner: Prof. Dr. Bart Gerritsen

Abstract

There has been a lot of research focused on the next generation of the internet, the so-called quantum networks. This analysis has been so far limited to mostly symmetrical architectures, but any near-term realisations of quantum networks using existing fibre topologies will contain asymmetry. In this thesis, we investigate how midpoint asymmetry affects quantum repeater protocols implemented with atomic ensembles. We extend the existing simulation framework to allow for midpoint asymmetry. By simulating asymmetry in elementary links, we show that the performance of an elementary link executing quantum key distribution decreases with an increasing degree of asymmetry. This effect can be mitigated by individual optimisation of photon sources at both ends of the elementary link. We present a way how to reduce the search space of such optimisations by developing a heuristic. The contributions of this thesis provide a crucial starting point for investigations of asymmetry in quantum repeater chains.

1 Introduction

The Internet has an unmistakable impact on our everyday lives. Quantum Internet, an extension of the classical internet using principles of quantum mechanics, has the potential to alter the world of technology. This potential of quantum technologies has been recognised by numerous countries and big technological companies [1], [2]. There are many exciting applications of Quantum Internet (such as Quantum Key Distribution [3] or Blind Quantum Computing [4]) that rely on fundamentally quantum mechanical properties and would not be attainable by classical communication alone.

In classical communication, when one wants to transfer information over a distance, classical bits are sent through a link. These classical bits can be amplified as necessary to counteract the effect of inherent losses in the channel. The amplification is implemented as making and sending a copy of the classical bit. It is impossible to directly apply this to quantum bits because quantum states cannot be copied due to the No Cloning Theorem [5, p. 532].

Transfer of quantum information instead relies on sharing **entangled states** between two places. Entanglement is a concept of quantum mechanics that is the foundation to realising novel applications and is defined at the beginning of Section 2. Efficient sharing of entanglement over large distances is one of the central challenges in the realisation of quantum networks. Lossy channels still pose a problem: locally creating a pair of entangled states and sending one of them to the destination is not a feasible approach because too much information about the state would be lost during the transmission. That is why quantum networks instead use protocols based on **quantum repeaters** [6]. These provide a promising solution for long-distance entanglement generation.

Quantum repeater protocols generate entanglement over sufficiently short **elementary links** which connect the end nodes through so-called repeater nodes as seen in Figure 1.1. Repeater nodes then perform entanglement swapping (see Section 2) to extend the distance over which entanglement is shared. Entanglement swapping is repeatedly carried out until there is shared entanglement over the total distance of the repeater chain. In this project, we are investigating solely elementary links.

The protocols we are considering are realised with **atomic ensembles and linear optics**. The first protocol that suggested using atomic ensembles and linear optics is called the DLCZ protocol after the authors Duan, Lukin, Cirac, and Zoller [8]. Since then, there have been many suggested improvements to the original protocol and the approach of implementing quantum repeaters with atomic ensembles appears to be promising [7]. More

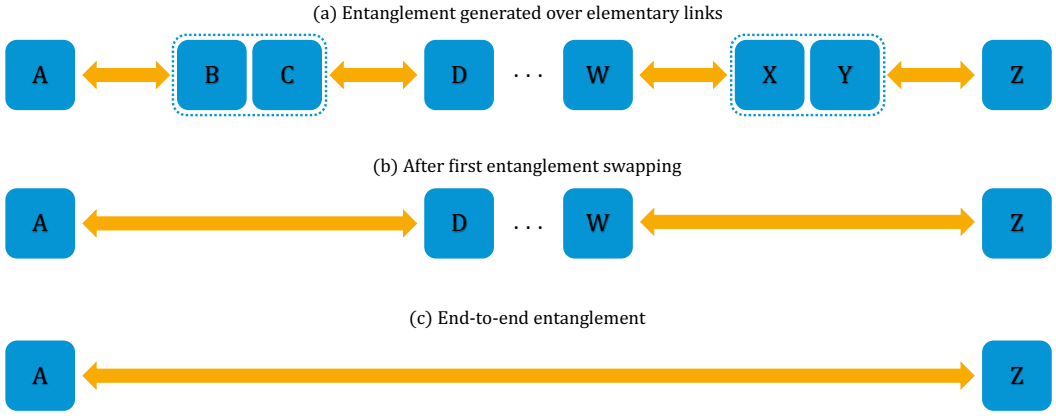

Figure 1.1: Principle of quantum repeaters [7]. Blue squares represent quantum memories and orange arrows depict shared entanglement. (a) Entanglement is first generated independently over elementary links, i.e. between neighbouring nodes. (b) Entanglement swapping is performed between neighbouring links. Entanglement swap at nodes B and C results in an entangled pair of states between A and D. (c) Entanglement is repeatedly swapped until there is end-to-end entanglement between the end nodes (here A and Z).

information about quantum repeaters and implementations based on atomic ensembles can be found in Section 2.

In the setup we are investigating, photons are used to generate entanglement over elementary links. At both ends of the elementary link, there is a node with a **probabilistic photon pair source**. Each photon pair source emits a pair of entangled photons: one is stored in the node's memory and one is sent through a channel to a midpoint station. The midpoint station detects incoming photons and performs a **Bell-state measurement** to generate entanglement between the nodes. A schematic of this setup is shown in Figure 1.2. The emission of photons is parameterised by the so-called **mean photon pair number** which tells us how many photons are emitted on average (see Equation (2.2)).

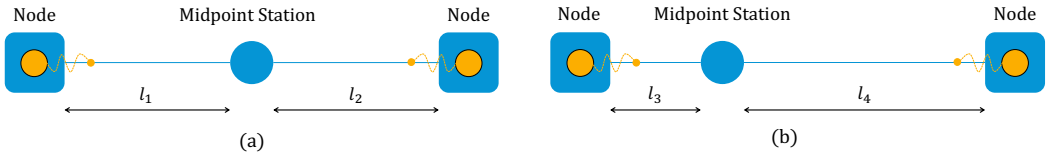

Figure 1.2: Elementary links between two nodes with (a) midpoint symmetry and (b) midpoint asymmetry. In this simplified scheme, nodes have probabilistic photon sources (orange circles) which emit photons and send them through fibres to the midpoint station. Bell-state measurements are performed at the midpoint station to generate entanglement between the nodes. The position of a midpoint station refers to how far it is placed from each side of the elementary link. In the case of symmetric midpoint placement (a) where $l_1 = l_2$, there is an equal amount of loss on both channels leading to the midpoint station. Midpoint asymmetry (b) where $l_3 \neq l_4$ leads to the non-trivial case of different losses on the two channels.

The specific scenarios we are investigating in this project are elementary links with **midpoint asymmetry**. Midpoint asymmetry means that the midpoint station is not placed

precisely in the middle of the elementary link (see Figure 1.2 (b)). The assumption of a symmetrical quantum network is often undertaken to simplify the investigations (for instance in [9]). However, using already existing fibre topologies to realise quantum networks will necessarily result in midpoint asymmetry because nodes in the fibre topologies are not equally spaced [10, Fig. 4.2]. An ongoing investigation that considers a case with midpoint asymmetry has shown asymmetry can have a significant effect on the optimal parameters of the hardware setup [11]. This indicates that a detailed analysis of the performance of asymmetric links will bear significantly different results than previous research that considered purely symmetrical networks. A detailed investigation of asymmetry is therefore necessary and will be the main goal of this project.

We analyse how midpoint asymmetry affects optimal parameters of DLCZ-inspired sources, specifically focusing on the value of mean photon pair number. Looking for the optimal value of the mean photon pair number is a non-trivial task. Higher values of mean photon pair number result in more photons being emitted, therefore increasing the entanglement generation rate. Because the emission is a probabilistic process, multiple photons are sometimes emitted at the same time which causes errors. The likelihood of multi-photon emissions increases with a higher mean photon pair number, in turn leading to higher errors. Therefore there is an optimal mean photon pair number at which the entanglement generation rate is high but at the same time the multi-photon emissions still do not cause significant errors; this is the value that results in the highest **secret key rate**. This parameter describes the rate at which secret key can be distributed (see Section 3.4 for its calculation) and it is the figure of merit we consider in our optimisations.

Simulation of quantum networks can be used to find how the mean photon pair number affects the performance. This is currently being investigated for symmetric cases [12]. Midpoint asymmetry has not been considered in any analysis so far and because the multi-photon emission errors are hard to treat analytically [13], there are no analytical results for this scenario as of now. The main goal of this project is to improve upon previous work by investigating the effects of midpoint asymmetry in detail.

We present three main contributions in this thesis:

- We extend the existing codebase for simulating quantum networks realised with atomic ensembles and linear optics to **support detailed physical modelling of midpoint asymmetry**. This provided framework is general enough to allow for the investigation of asymmetry in repeater chains but such analysis is outside the scope of this project.
- We show that **midpoint asymmetry has a significant effect on performance of elementary links**, specifically on the highest achievable value of secret key rate.
- We analyse how **individual optimisation of mean photon pair number** for sources at both end nodes of an elementary link **helps to mitigate the effects of midpoint asymmetry** and present a way to reduce the search space of such optimisations.

The rest of this thesis is structured as follows: Section 2 offers background information about the physics behind the protocols we consider. Section 3 describes the details of simulating quantum networks, discusses how asymmetry is included in our simulations, and motivates the choice of simulation parameters. Section 4 shows the results of simulations for varying degrees of asymmetry. In Section 5, replicability of this investigation is discussed.

Section 6 summarises the conclusions of this project and suggests concrete ideas for future investigations.

2 Background Information

In this section, we illustrate what entanglement means and how is it used to realise quantum networks. Furthermore, we motivate the choice of protocols that are being investigated in this project. This section contains background information from a physics perspective but understanding the details presented here is not a requirement for following the rest of the paper.

Before we describe the protocols based on atomic ensembles, we need to explain what entanglement is. Entanglement is a fundamental concept in quantum mechanics and allows for many interesting applications. It is central to the distinction between classical and quantum physics because it does not have an equivalent in classical mechanics. If two states are entangled, the state of one particle cannot be described independently without the state of the other particle. To illustrate this concept, we give an example of a special case of entanglement – a maximally entangled Bell state of two qubits from systems A and B:

$$|\psi^+\rangle = \frac{1}{\sqrt{2}}\big(|0\rangle_A \otimes |1\rangle_B + |1\rangle_A \otimes |0\rangle_B\big) \tag{2.1}$$

Equation (2.1) represents a superposition of the probabilities that the state of system A is 0 and the state of system B is 1 and vice versa. If Alice were to measure system A in the $\{|0\rangle, |1\rangle\}$ eigenbasis, the system would collapse to either $|0\rangle_A \otimes |1\rangle_B$ or $|1\rangle_A \otimes |0\rangle_B$ depending on the outcome of Alice's measurement (which would be 0 or 1 respectively). Any measurement performed by Bob on system B would then be anti-correlated with Alice's measurement; it would always be a different measurement outcome than what Alice measured (1 or 0 respectively). Entanglement is a crucial property that allows for implementing quantum networks using quantum repeater protocols.

The concept of quantum repeaters is an alternative to classical signal amplification. Amplification of quantum information is impossible because of the No Cloning Theorem [5, p. 532] and instead protocols based on quantum repeaters are used to realise quantum networks [6]. A repeater chain can be seen in Figure 1.1 (a) where the dotted square around two quantum memories depicts a repeater node. Repeater nodes are placed between two end nodes to divide the total length between two end nodes into elementary links; placing N repeater nodes means creating $N + 1$ elementary links. Elementary links are used for entanglement generation at a smaller distance over which the losses on the fibre are not significant yet. The generated entanglement is then repeatedly swapped between neighbouring links by performing Bell-state measurements to obtain a shared entanglement over the total distance.

The DLCZ protocol realises a quantum repeater scheme with atomic ensembles and linear optics [8]. The DLCZ protocol makes use of spontaneous Raman emission: at each node, there is an atomic ensemble that emits a photon and creates a spin-excitation entangled to the emitted photon. The emitted photons are sent to a midpoint station where a Bell-state measurement is performed. The Bell-state measurement projects the state of the two end nodes onto a maximally entangled state (Bell state). Bell-state measurements using linear optics can make projections on two out of the four Bell states, introducing an upper limit of 50 % for the success probability of the measurements. The result of this measurement is

classically sent back to the end nodes and in this way, entanglement is generated over the elementary link.

When considering the DLCZ scheme, shared entanglement is based on a single excitation in one of the end nodes. The Bell-state measurement at the midpoint station is performed by a beam splitter and single-photon detectors. The measurement is done in a way that destroys the which-way information, making the detection of a single photon in one of the detectors a successful **heralding event** [7] which confirms that there is a delocalised excitation in one of the atomic ensembles. The only measurements that can be performed on a single-photon entanglement are in the Fock basis $\{|0\rangle, |1\rangle\}$; these are measurements of the number of excitations. This constraint limits the number of possible uses. To be able to measure in an arbitrary basis, we need to generate two-photon entanglement for which two individual elementary links are required, each with a single delocalised excitation. More information on how this is implemented and how it affects the post-selection can be found in Section 3.1.

In the original DLCZ protocol, the atomic ensemble acts as both a source and a memory at each node; we consider the probabilistic photon source and the memory to be one component. We parameterise such a source by the so-called mean photon number. The DLCZ setup can be also modelled by a separation of the source and the memory. In that case, the source is a probabilistic photon *pair* source because one of the emitted photons is stored in the memory and one is sent over a channel to the midpoint station. We can describe the source by a parameter called mean photon *pair* number. Both the mean photon number and the mean photon number can be expressed by the same equation

$$\mu = \sum^{n} n \cdot p(n), \tag{2.2}$$

where μ is the mean photon (pair) number, n is the number of emitted photons (photon pairs), and $p(n)$ is the probability of emitting n photons (photon pairs). Whether n denotes the number of photons or the number of photon pairs does not affect the underlying physics. In the rest of the paper, we use the term mean photon pair number because we model the DLCZ setup with a separation of the source and the memory. This has several advantages, most importantly greater flexibility of wavelengths of emitted photons and an easier improvement of the protocol by an approach called **multiplexing**. Multiplexing utilises some degree of freedom to create different modes in which photons can be sent. This can, for example, be spectral (sending photons with different frequencies), temporal (sending photons in different time windows), or spatial (sending photons in different locations).

Multiplexing increases the rate at which entanglement can be generated because there are more possibilities for entanglement generation as photons can be sent in different modes [14]. Protocols using probabilistic photon pair sources and multiplexing (such as [14]) are promising candidates for realising repeater chains due to the improved entanglement generation rate and have been the focus of many experimental efforts [7]. It is therefore interesting to see how these protocols would behave if they were used in realistic fibre topologies; topologies that will undoubtedly be asymmetric [10, Fig. 4.2].

There are two possibilities of asymmetry due to the topology: (a) different lengths of elementary links within a repeater chain due to asymmetric placement of repeater nodes (repeater asymmetry) and (b) different lengths of channels going from the nodes to a midpoint station due to asymmetic placement of midpoint stations (midpoint asymmetry). We are considering only elementary links in this project, therefore we focus solely on the latter case of midpoint asymmetry. We define midpoint asymmetry as

$$A = \frac{|l_1 - l_2|}{l_1 + l_2}, \tag{2.3}$$

where l_1 is the channel length between the left node and the midpoint station and l_2 is the channel length between the midpoint station and the right node [15]. We choose this specific definition because it has several convenient properties: the value of asymmetry is 0 when the midpoint placement is completely symmetric and the absolute value in the definition abstracts away whether the midpoint station is placed closer towards the left or right side of the elementary link. This reduces the number of possible midpoint station placements we need to consider in order to investigate the effect of midpoint asymmetry. In this project, we vary the midpoint station placement in the left half of an elementary link. Another feature of the definition above is that it is easily extendable to repeater chains with both midpoint and repeater asymmetry by defining two separate values of A for the two types of asymmetry. This is outside the scope of this project but provides a possibility of unified notation in future investigations.

3 Simulations

Analytical treatment of multi-photon emission errors is non-trivial [13] and employing simulations to investigate these scenarios has proven to be an effective approach [9], [12]. In this section, we explain the setup of our simulations and how the investigated protocol is modelled.

The simulator used in this project is the **Net**work **S**imulator for **Qu**antum **I**nformation using **D**iscrete events (NetSquid) [16]. For more detailed information about how the components such as the sources, memories, and detectors are modelled in NetSquid, see [9]. To allow for midpoint asymmetry, new additions to the codebase were implemented and these are explained in detail in Section 3.3.

3.1 Protocol

The protocol we are investigating is the DLCZ protocol [8] but with an adjustment that separates the source and the memory into individual components. The DLCZ protocol uses single-photon detectors. The detectors herald success when they detect a single "click", i.e. an arrival of one photon. A single click at the detector can also be caused by multiple photons that cannot be distinguished.

The states are in presence-absence encoding as the only available information is whether the photon is present ($|1\rangle$) or absent ($|0\rangle$). In our simulations, we define which states can be sampled from the source component by defining a distribution for the sampling. In the case of presence-absence encoding, the distribution is taken from [17, eq. (2.19)].

As briefly discussed in Section 2, the entanglement that can be shared between two nodes running a single-click protocol is not useful for computations which is why we need two parallel elementary links in a so-called dual chain. Such a setup can be seen in Figure 3.1 and it creates a more useful two-photon entanglement that allows for measurements in any basis. In our case, the Bell-state measurements at the end nodes are performed in the X and Z basis. Depending on the measurement basis, a different setup of the Bell-state measurement is used. In the Z basis, the incoming states are directly measured. In the X basis, the states are first interfered on a beam splitter.

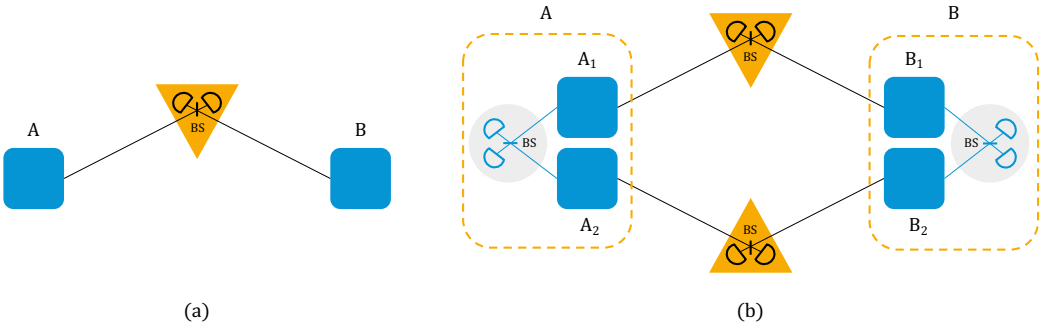

Figure 3.1: Scheme of (a) an elementary link and (b) a dual chain of elementary links. In the dual chain, entanglement is first independently generated on the $A_1 - B_1$ and $A_2 - B_2$ links using Bell-state measurements (orange triangles) with a beam splitter (BS) and single-photon detectors. By reading out the states on both sides (denoted by dashed squares) of the setup through a Bell-state measurement (grey circles), two-photon entanglement is generated.

When entanglement is established on both elementary links, post-selection is applied in which the states on both sides of the dual chain are read out and two-photon entanglement is generated. During the post-selection, some rounds must be discarded. This is because sometimes both photons from the generated two-photon entanglement reside on the same end of the dual chain (e.g. in A_1 and A_2 in Figure 3.1). We can determine this situation occurred when both nodes on one end of the dual chain have the same measurement outcome in the Z basis.

3.2 Runtime Optimisation

There are multiple ways how to run the simulations and these can be divided into two categories: running the full simulations and using so-called *magic* to speed up the process. The different components and individual protocols used in both cases are shown in Figure 3.2. The general workflow of one round of the simulation is as follows: the source on each node emits a state and sends it to the detector at the midpoint station, the midpoint station performs a Bell-state measurement, and the results are classically communicated back to the nodes.

In the case of a full simulation, the clock ticks at specified time intervals which causes `EmissionProtocol` to trigger the source. The source randomly samples a state from the full density matrix. The density matrix allows calculation of the probabilities and the corresponding measurement outcomes for an entangled system. The sampled state is sent to the midpoint station. This is a probabilistic process; a low value of mean photon pair number reduces the multi-photon emission errors but results in a lot of samples that are vacuum and do not result in a state. To speed up the runtime of the simulation, we use *magic*.

Magic is a term used within the codebase and refers to the fact that we sample the full end-to-end state of the elementary link after a successful Bell-state measurement and "magically" put this state into the memory. In this way, we skip all unsuccessful rounds (due to producing vacuum or due to an unsuccessful Bell-state measurement) and consider only successful rounds.

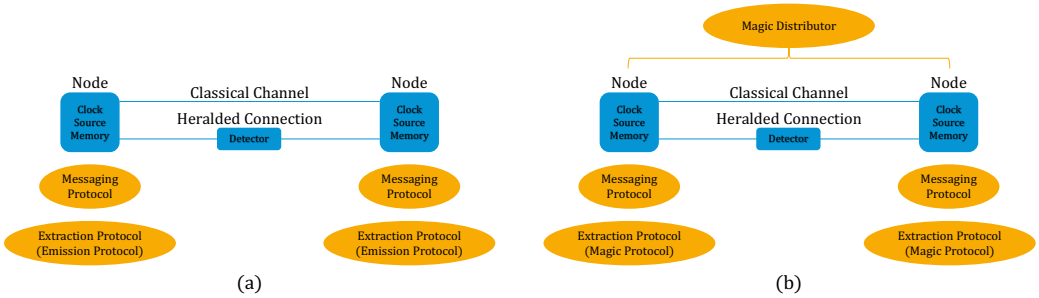

Figure 3.2: Simulation setup for (a) simulations without *magic* and (b) simulations with *magic*. Components modelling hardware are depicted as blue squares and protocols are shown as orange ovals. The striking difference between the two setups is the `MagicDistributor` which handles state and label deliveries.

To be able to use *magic*, we first run the full simulation for every successful midpoint detector outcome. For the presence-absence encoding, there are exactly two successful outcomes corresponding to a click from either the left or the right side of the elementary link. A sample file is created with the full end-to-end states which is then used in subsequent simulations. `MagicDistributor` calculates the probability with which entanglement is successfully generated and directly skips to the next successful round. `MagicDistributor` then distributes states sampled from the sample file to memories on both nodes and delivers labels with measurement outcomes the nodes would receive from the midpoint station. This significantly speeds up the simulations because we only consider rounds where there is no vacuum and the Bell-state measurement is successful.

3.3 Midpoint Asymmetry

Investigating midpoint asymmetry is the focus of this project. Accounting for such scenarios in the simulations can provide valuable insight into the optimal setup of hardware for quantum networks. Implementing midpoint asymmetry required adjustments to three components in the simulation: `HeraldedConnection`, `EmissionProtocol`, and `MagicDistributor`. `HeraldedConnection` holds a detector and channels between the nodes and the detector; to allow for midpoint asymmetry, we simply have to allow for different channel lengths. The necessary changes in the other two components are explained in this subsection.

`EmissionProtocol` is used when the full simulation is run. The protocol runs on each node and is triggered by clock ticks. At each clock tick, the protocol triggers the source at the node to emit a state. However, when the channels going to the midpoint station have different lengths, the states take different time to travel to the midpoint station. A Bell-state measurement at the midpoint station can only happen successfully if states arrive at the same instant, hence the necessary change in `EmissionProtocol` includes allowing for a delayed trigger of the source. In elementary links with midpoint asymmetry, only one of the emission protocols needs to have a delay. The delay is calculated as $|l_1 - l_2|/c$ where c is the fixed speed of photons through the channel in km/s.

`MagicDistributor` handles state and label deliveries; state delivery replaces state being put into the memory and label delivery replaces receiving the measurement outcome from the midpoint station. Delays for both types of deliveries depend on the channel lengths.

States need to be put onto memories such that they would arrive at the midpoint station in the same instant and labels need to be delivered at the same time as well. In a completely symmetric case, the delay for states is 0 and the delay for labels is a value of **cycle time**. Cycle time (see Equation (3.1) where c is again the fixed speed of photons through the channel in km/s) is the time it takes a state to travel to the midpoint station and a classical message to travel back to the node. In the case of midpoint asymmetry, state and label delays are different for the left and right channels, see the calculation in Equations (3.2) and (3.3).

$$\texttt{cycle\_time\_(l/r)} = \frac{\texttt{channel\_length\_(l/r)} * 2}{c} \tag{3.1}$$

$$\texttt{state\_delay\_(l/r)} = max(\texttt{cycle\_time\_l}, \texttt{cycle\_time\_r}) - \frac{\texttt{cycle\_time\_(l/r)}}{2} \tag{3.2}$$

$$\texttt{label\_delay\_(l/r)} = max(\texttt{cycle\_time\_l}, \texttt{cycle\_time\_r}) - \texttt{state\_delay\_(l/r)} \tag{3.3}$$

The biggest challenge of these implementations stems from the fact that NetSquid is a discrete-event simulator and allows for the study of time-dependent noise [16]. The timing in the simulations is crucial and allowing for midpoint asymmetry complicates the existing simulation framework. Furthermore, this project also necessitated the creation of a simulation script that allows for easy variability of degrees of asymmetry of elementary links and the mean photon pair number for both sources. Development of the framework and the simulation script are contributions that can be useful in future investigations.

3.4 Data Collection

The figure of merit we are considering when searching for the value of the optimal mean photon pair number is called **secret key rate** (SKR). In our case, this describes the rate at which a secret key can be distributed using the BB84 protocol [3] and takes into consideration both the entanglement generation rate as well as the quality of the created state. To explain how SKR is calculated, we first need to define two parameters we extract from the simulation data: rate of success and quantum bit error rate (QBER).

Rate of success R_{SUCC} is the rate at which entanglement is successfully generated between the end nodes. In the data collected from our simulations, the unit used for the rate is not a unit of time but rather an attempt at entanglement generation. If we used time for the rate of success, it would be possible to arbitrarily affect that by seting the time intervals on which the clocks tick. Instead, one round of the simulation (i.e. one attempt at entanglement generation) reflects the probabilistic processes in our simulations. We express rate of success as $1/\texttt{attempts\_per\_success}$ where `attempts_per_success` denotes the average number of attempts required for successful entanglement generation.

QBER is calculated from the measurement outcomes; it is the fraction of wrong bits in the total number of successful measurements. A low value of QBER means having a state with higher quality. QBER is determined individually for the X and Z bases in which the measurements are performed. The number of wrong bits is determined by comparing the end node measurements to the expected outcomes. For Z basis, we always expect the results to be anti-correlated. In the X basis, the expected outcome depends on the outcome of the measurement at the midpoint station.

Having defined rate of success R_{SUCC} and QBER in both the X and Z basis, the corresponding value of secret key rate is calculated as

$$SKR = R_{SUCC} \times max(0, 1 - H(\text{QBER}_X) - H(\text{QBER}_Z)), \tag{3.4}$$

where $H(p)$ is the binary entropy function defined as $H(p) = -p \log_2 p - (1-p) \log_2 (1-p)$.

We run the simulations for varying values of mean photon pair number and determine R_{SUCC} and QBER for each of the data points. We fit a polynomial to these values and sweep over a range of mean photon pair numbers, calculating the resulting value of the secret key rate for each of them. The optimal mean photon pair number is then the value that results in the highest value of SKR.

3.5 Choice of Parameters

The simulation framework models all of the components in the elementary link. There are more input parameters than the parameters needed to be considered in this investigation: some are describing components we do not directly focus on (e.g. the midpoint detectors) and some offer variability in the kind of protocol the simulation is running (e.g. different encoding or the number of modes for multiplexing). The parameters for individual components will certainly affect the resulting values of the secret key rate, nonetheless, we expect the trend of the optimal mean photon pair number to stay the same. For example, if we introduced imperfect detectors into our simulations, the QBER would be higher and values of SKR would drop. This source of noise would in that case be independent of the degree of midpoint asymmetry. The choice of exact values of such parameters is to some extent arbitrary, so we consider the simplest scenario with only two sources of noise. These are fibre attenuation and errors resulting from multi-photon emission; the effect of both of these sources of noise is dependent on the particular degree of asymmetry. All the other parameters are set to perfect values and can be found in Appendix A.

4 Results

After having explained all relevant aspects of the simulations, we now present the results of our analysis of the effects of midpoint asymmetry on elementary links. As explained in Section 1, we expect the mean photon pair number to have an optimal value. This optimal value is determined as the value that results in the highest secret key rate. The reasoning behind this is that higher values of mean photon pair number lead to increased entanglement generation rate which is in turn reflected in higher values of SKR. However, increasing the mean photon pair number also causes multi-photon emission errors which have a negative effect on the quality of the created state resulting in lower values of SKR.

The first simulation results we show in Figure 4.1 compare plots of SKR, QBER and entanglement generation duration for two elementary links – one with midpoint symmetry and one with midpoint asymmetry. The unit of entanglement generation duration is the average number of attempts per successful entanglement generation (see Section 3.4). We look in detail at these two sets of plots to verify that the mean photon pair number has an optimum (as explained above) and to describe how we extract the highest achievable value of SKR from the simulation data.

We observe in Figure 4.1 that varying the mean photon pair number leads to the expected behaviour of SKR for both degrees of asymmetry, where the SKR first increases with

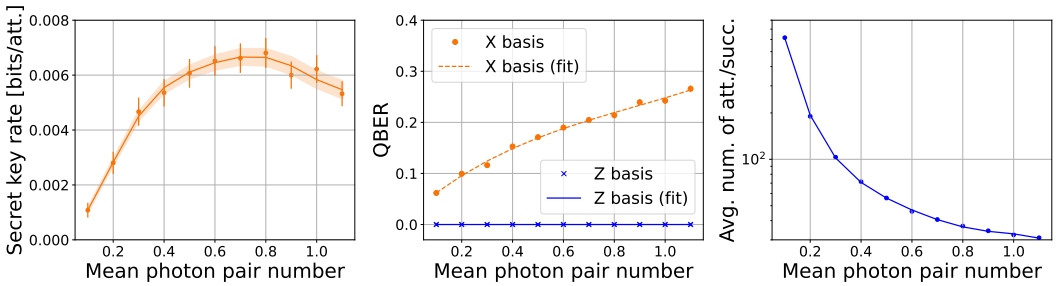

(a) $A = 0$

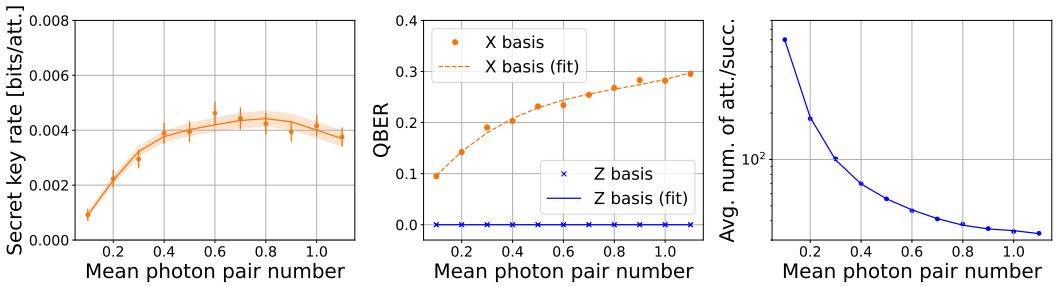

(b) $A = 0.5$

Figure 4.1: Results for elementary links with total length of 50 km for two different values of asymmetry $A = 0$ (fully symmetric case) and $A = 0.5$. Simulations are in presence-absence encoding. For each value of mean photon pair number, the simulation is run until there are 10000 successful entanglement generation attempts. Values of QBER and entanglement generation duration are fitted with polynomials and the fit for SKR is calculated according to Equation (3.4). The shaded areas around the trendline for the values SKR represent the confidence intervals. Lengths of channels between the nodes and the midpoint station can be calculated from Equation (2.3): (a) both channels are 25 km long, (b) the left channel is 12.5 km and the right channel is 37.5 km long.

increasing mean photon pair number but then after a clear maximum decreases due to the dominant effect of multi-photon emisssion errors. We see that the maximal obtained values of SKR are significantly lower for the elementary link with midpoint asymmetry. This shows that midpoint asymmetry affects the achievable values of SKR. The QBER in the X basis increases when the channels have different lengths, meaning the quality of the created state decreases when asymmetry is introduced to the elementary link. QBER in the Z basis is always 0 because we assume the detectors at the midpoint station are perfect; no click is registered unless there is an incoming photon. Due to the post-selection of dual chain elementary links where we only keep results with one excitation per node (see Section 3.1), we never get a result that would produce a non-zero QBER in the Z basis.

The shaded areas represent the confidence intervals for values of SKR. The lower and upper bound is obtained by calculating the value of SKR according to Equation 3.4 for highest QBER and lowest rate, and lowest QBER and highest rate respectively. To obtain the highest possible value of SKR, we find the maximum of the fit to SKR and use the confidence interval as an error bar. Highest valued of SKR for varying degrees of asymmetry can be seen in Figure 4.2.

The first trend that is immediately apparent as shown in Figure 4.2 is that the highest

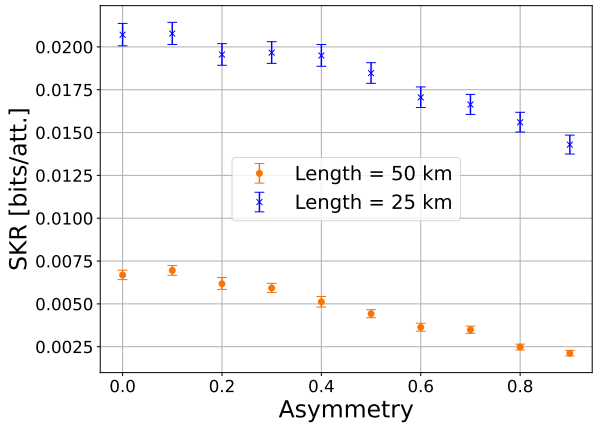

Figure 4.2: The maximum value of SKR obtained for varying degrees of midpoint asymmetry for two different elementary links with total lengths of 25 km and 50 km. The simulations are in presence-absence encoding and are run for 10000 successful entanglement generation attempts. The left channel is always the shorter channel. Midpoint asymmetry results in lower values of SKR. More losses are introduced on the longer elementary link, leading to consistently lower values of SKR.

value of SKR decreases as the elementary links get more asymmetric. We show this result for two different lengths of elementary links, suggesting this behaviour will be observable for arbitrarily long elementary links. The reason why the values of SKR are consistently lower for the longer elementary link is that more losses are introduced to the states travelling through longer fibres. These losses are caused by the fibre attenuation.

All the plots that we used to extract the maximum values shown in Figure 4.2 can be found in Appendix B. From these plots, we can see that the optimal value of the mean photon pair number (the one corresponding to the highest value of SKR) has no observable trend and is usually found to be around 0.8. We believe the reason for this is that the optimal value diverges for both sources and when we assume both sources have the same mean photon pair number, there is no resulting observable upwards or downwards trend. This diverging behaviour can be indeed observed in Figure 4.3 as we will explain later.

Allowing for asymmetrical values of mean photon pair number for sources on both nodes in the elementary link quadratically increases the search space. We consider the probability of a photon arriving at the midpoint station as a means of reducing the size of the search space. This probability can be calculated as

$$\mu \times \tau(L) = \mu \times 10^{-\alpha L/10}, \tag{4.1}$$

where μ is the mean photon pair number of the source, α is the fibre attenuation in dB/km, and L is the length of the fibre between the node and the midpoint station. $\tau(L)$ denotes the **transmittance**, i.e. the probability of transmitting a photon over a given length. The probability of a photon arriving at the midpoint station can be calculated separately for each side of the elementary link, we denote the two values as p_l and p_r for the left and right side respectively.

The highest values of SKR are obtained when the elementary link is completely symmetric. When we assume that the values of mean photon pair numbers are the same for both

nodes, $p_l = p_r$ for a symmetric elementary link. However, if we maintain the assumption of symmetric mean photon pair numbers and introduce midpoint asymmetry, p_l does not equal p_r anymore. This further motivates the investigation of asymmetric mean photon pair numbers because it would allow for situations where $p_l = p_r$ even if a link contains midpoint asymmetry. Figure 4.3 shows resulting values of SKR for a setup with asymmetric mean photon pair numbers. For each degree of asymmetry, we show a line where the probability of photons arriving at the midpoint station is equal to see whether it crosses the area in the graph where the highest values of SKR are observed.

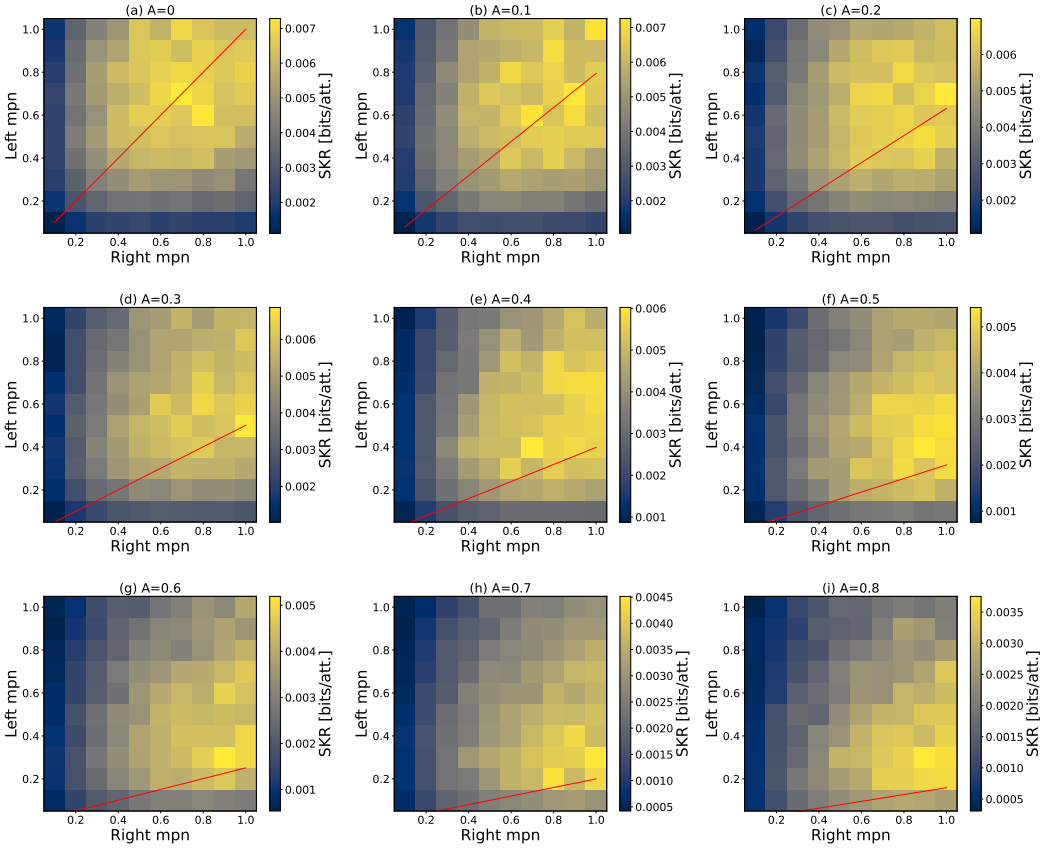

Figure 4.3: Obtained value of SKR for varying degrees of asymmetry when we allow the sources to have different mean photon pair numbers. The red lines show combinations of mean photon pair numbers that result in $\mu_l \times \tau(L_l) = \mu_r \times \tau(L_r)$. Note that the scales of SKR are different for each plot such that we can clearly see where the highest value of SKR can be observed. In these simulations, the left channel is always the shorter one. It is clear that as the left channel gets shorter, the optimal value of the left mean photon pair number decreases. There is a fairly consistent agreement between the highest values of SKR and the areas where probabilities of photons arriving at the midpoint station are the same.

Figure 4.3 clearly shows that the optimal values of mean photon pair number for both sources diverge with asymmetric elementary links. The heuristic $p_l = p_r$ approximately follows the trend of diverging mean photon pair numbers. Note that there are no error

bars depicted in Figure 4.3 and the data shown are exact values from simulation data. For higher degrees of asymmetry, the heuristic does not seem to precisely cross the area with the highest values of SKR. Reducing the search space for the case of asymmetric mean photon pair numbers is crucial for further investigation of midpoint asymmetry, therefore we keep using the heuristic. We only consider combinations that satisfy $\mu_l \times \tau(L_l) = \mu_r \times \tau(L_r)$ (where l and r refer respectively to the left and right side of the elementary link) for a certain degree of asymmetry. This reduces our search space and we are able to obtain simular plots as in Figure 4.1. We therefore compare a setup where both sources must have the same mean photon pair number with a setup where the mean photon pair number of both sources can be individually optimised. This is depicted in Figure 4.4. All plots used to extract the highest value of SKR for case of asymmetric mean photon pair numbers can be found in Appendix C.

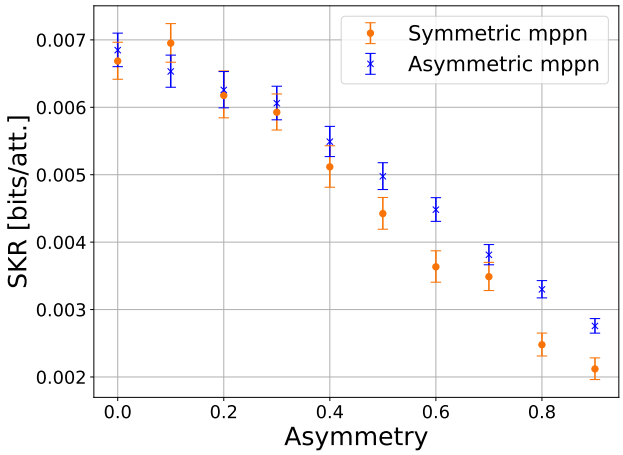

Figure 4.4: The highest value of SKR obtained for varying degrees of midpoint asymmetry in elementary links with symmetric and asymmetric values of mean photon pair numbers at both sources. The simulations are in presence-absence encoding and are run until there are 10000 successes of entanglement generation. The left channel is always the shorter channel. Allowing for asymmetric values of mean photon pair numbers results in higher values of SKR.

Figure 4.4 shows that individual optimisation of the two sources results in higher values of SKR. The values of SKR for asymmetric mean photon pair numbers are consistently higher starting from values $A = 0.4$. For lower degrees of asymmetry, the error bars for symmetric and asymmetric mean photon pair numbers overlap. Specifically at $A = 0.1$, we see that the maximum value of SKR is higher for the case of symmetric mean photon pair numbers. We do not expect this to reflect any underlying behaviour. We observe a clearer distinction between obtained values of SKR for higher degrees of midpoint asymmetry which suggests that allowing for asymmetric mean photon pair numbers causes significant improvement in obtained values of SKR only for more asymmetric elementary links. We conclude that using the investigated heuristic $\mu_l \times \tau(L_l) = \mu_r \times \tau(L_r)$ results in better performance of highly asymmetrical elementary links even though we do not have enough data to conclude if this heuristic results in the optimal values of mean photon pair numbers. This nevertheless shows that the effect of midpoint asymmetry can be to some extent mitigated by parameters optimised individually for each of the nodes in an elementary link.

5 Responsible Research and Discussion

Doing research responsibly is an obligation that comes with the privilege of being a scientist. In this context, it is crucial that this project can be replicated and the results can be verified. To ensure replicability, two aspects of this project need to be considered: the code used to run the simulations and the obtained data.

Firstly, the code for all the components in the simulation is available on a public repository as a snippet [18]. There are several dependencies of this project and all of them are accessible to the public as well, including the software tool for modelling and simulating quantum networks called NetSquid [16]. Secondly, the obtained data (both raw and processed) is stored in a repository. This data will be available upon request to anyone who wishes to replicate the results. This repository also contains the scripts for simulation, processing and plotting along with instructions on how to run them.

The simulations have a lot of input parameters which can significantly affect the obtained data. Parameters that were not varied during this project can be found in Appendix A. The repository with all the data from this project also contains files with the used parameters. It is also important to note that the simulations are probabilistic in nature but the behaviour shown in this paper can be replicated with a sufficiently large number of runs.

Additionally, it is worthwhile to assess whether the obtained results agree with previous work. As mentioned in Section 1, there has been no analysis focusing specifically on effects of midpoint asymmetry in atomic ensemble based quantum repeater protocols. Nevertheless, we confirm that the findings of this thesis agree with preliminary results from two projects that use NetSquid simulations to study the performance of quantum networks. One of these projects is focusing on atomic ensemble based repeater protocols [12] and demonstrates the same behaviour of secret key rate in response to varying mean photon pair number as we did in Figure 4.1 but for single repeater setups. The second project considers a single repeater setup with repeater and midpoint asymmetry, albeit not for atomic ensemble based protocols [11]; preliminary results from this research suggest that midpoint asymmetry has a negative impact on the performance of quantum networks which we confirm with our findings.

6 Conclusions and Future Research

In this section, we present some concrete ideas for future investigations into the topic of asymmetry in atomic ensemble based quantum repeater protocols. First, we briefly summarise what we did in this thesis and which conclusions we reached.

In the previous sections, we investigated the effect of mipoint asymmetry on the performance of elementary links implemented with the DLCZ setup. To do this, we extended an existing simulation framework to allow for scenarios with midpoint asymmetry. Using these simulations, we showed that midpoint asymmetry negatively affects the highest achievable values of secret key rate in elementary links. We then improved upon these obtained values of secret key rate by allowing for asymmetric mean photon pair numbers. Allowing both sources in an elementary links to have different mean photon pair numbers significantly increased the search space, so we devised a simple heuristic that can predict which combinations of mean photon pair numbers might result in a better performance than symmetric mean photon pair numbers. This heuristic did not fully capture the trends shown in our simulation data but nonetheless resulted in higher obtained values of secret key rate than in the case of symmetric mean photon pair numbers.

In this project, we argued that there is no observable trend in the optimal mean photon pair number when we assume both sources at the end nodes of an elementary link have the same mean photon pair number. We clearly showed that this is not the case for asymmetric mean photon pair numbers because we observed that the optimal values of the mean photon pair number diverge. A convenient extension to the investigations of this thesis would be to devise a way how to extract the optimal value of mean photon pair number and its uncertainty, for both symmetric and asymmetric mean photon pair numbers. This would allow us to plot the optimal values for varying degrees of asymmetry and investigate the trends in more detail.

To find the highest value of secret key rate, we ran the simulations and fitted a polynomial to the QBER and entanglement generation duration data extracted from the simulations. We then calculated the corresponding value of secret key rate for varying degrees asymmetry and performed a parameter scan to find the highest values of secret key rate. This is the most straighforward way of finding the highest values of SKR but employing a more sophisticated optimisation algorithm would lead to more robust results. This could also prove to be an effective way of obtaining the optimal values of mean photon pair numbers with clearer approaches of calculating their uncertainties.

We purposefully limit the sources of noise in our simulations to the multi-photon emission erros and the fibre attenuation. To further investigate noise in the simulations, imperfect detectors could be introduced which would result in non-zero values of QBER in the Z basis. Considering more sources of noise such as imperfect detectors would bring us one step closer towards realistic scenarios.

Another possible extension is to investigate repeater and midpoint asymmetry in repeater chains. The definition of asymmetry used in this thesis supports both midpoint and repeater asymmetry, allowing for a unified notation in repeater chains. Investigating asymmetry in repeater chains is a step closer towards realistic scenarios and would surely lead to useful results. We can also expect the results for repeater chains to be different than for elementary links in terms of quality of the created state. While entanglement generation over elementary links in a repeater chain is investigated by the simulations in this thesis, entanglement swapping introduces more operations leading to a higher QBER.

The findings of this project show that the results for asymmetric scenarios are significantly different than for symmetric ones. Asymmetry will undoubtedly play an important role in quantum networks due to existing asymmetries in fibre topologies. That is why investigation of the effects of asymmetry, both midpoint and repeater, is beneficial for near-term realisations of quantum networks. This thesis provides a solid stepping stone for future research of asymmetry in quantum repeater chains.

Acknowledgments

Firstly, I would like to thank all the committee members: Prof. Stephanie Wehner, Prof. Bart Gerritsen and David Maier. I am very grateful to Prof. Stephanie Wehner for allowing me to do my thesis in her group; you have been a great inspiration, and I am so thankful for the doors you have opened for me. Furthermore, I would like to thank my supervisor David for his guidance, invaluable feedback and patience with my endless questions. I could not have wished for a better supervisor. The members of the blueprint team have also contributed to making this project a remarkable learning experience; my gratitude goes to Guus, Francisco, Tim, Emlyn, and Luc for their helpful remarks. Finally, I would like to thank my parents and my brother for their unconditional support.

References

[1] Anonymous. "EU-funds quantum technology projects," Horizon 2020 - European Commission. (Jan. 29, 2016), [Online]. Available: https://ec.europa.eu/programmes/horizon2020/en/news/eu-funds-quantum-technology-projects (visited on 06/24/2021).

[2] "Quantum delta NL awarded 615 million euro from netherlands' national growth fund to accelerate quantum technology," Quantum Delta NL. (Apr. 9, 2021), [Online]. Available: https://quantumdelta.nl/quantum-delta-nl-awarded-615-million-euro-from-netherlands-national-growth-fund-to-accelerate-quantum-technology-2/ (visited on 06/24/2021).

[3] C. H. Bennett and G. Brassard, "Quantum cryptography: Public key distribution and coin tossing," en, *Theoretical Computer Science*, vol. 560, pp. 7–11, Dec. 2014, ISSN: 03043975. DOI: 10.1016/j.tcs.2014.05.025. [Online]. Available: https://linkinghub.elsevier.com/retrieve/pii/S0304397514004241 (visited on 06/07/2021).

[4] A. Broadbent, J. Fitzsimons, and E. Kashefi, "Universal blind quantum computation," *arXiv:0807.4154 [quant-ph]*, Dec. 12, 2009. DOI: 10.1109/FOCS.2009.36. arXiv: 0807.4154. [Online]. Available: http://arxiv.org/abs/0807.4154 (visited on 06/16/2021).

[5] M. A. Nielsen and I. L. Chuang, *Quantum Computation and Quantum Information*. Cambridge University Press, 2010, ISBN: 9781107002173.

[6] H. J. Briegel, W. Dür, J. I. Cirac, and P. Zoller, "Quantum repeaters: The role of imperfect local operations in quantum communication," *Physical Review Letters*, vol. 81, no. 26, pp. 5932–5935, Dec. 1998, ISSN: 10797114. DOI: 10.1103/PhysRevLett.81.5932. [Online]. Available: https://journals.aps.org/prl/abstract/10.1103/PhysRevLett.81.5932.

[7] N. Sangouard, C. Simon, H. de Riedmatten, and N. Gisin, "Quantum repeaters based on atomic ensembles and linear optics," *Reviews of Modern Physics*, vol. 83, no. 1, pp. 33–80, Mar. 2011. DOI: 10.1103/RevModPhys.83.33. arXiv: 0906.2699. [Online]. Available: http://arxiv.org/abs/0906.2699%20https://link.aps.org/doi/10.1103/RevModPhys.83.33.

[8] L. M. Duan, M. D. Lukin, J. I. Cirac, and P. Zoller, "Long-distance quantum communication with atomic ensembles and linear optics," *Nature*, vol. 414, no. 6862, pp. 413–418, Nov. 2001, ISSN: 00280836. DOI: 10.1038/35106500. [Online]. Available: https://www.nature.com/articles/35106500.

[9] D. Maier, "Investigating the Scalability of Quantum Repeater Protocols Based on Atomic Ensembles," Master's Thesis, Ludwig-Maximilians-Universität Munich, Munich, Mar. 2020.

[10] J. Rabbie, "Simulation Model for Atomic Ensemble based Quantum Repeaters and the Optimization of their Positioning," Master's Thesis, Delft University of Technology, Delft, Jan. 2020. [Online]. Available: http://resolver.tudelft.nl/uuid:d687b10f-3948-4185-9418-53044e15c0ab.

[11] G. Avis, D. Maier, and F. Silva, In preparation, 2021.

[12] D. Maier, In preparation, 2021.

[13] S. Guha, H. Krovi, C. A. Fuchs, Z. Dutton, J. A. Slater, C. Simon, and W. Tittel, "Rate-loss analysis of an efficient quantum repeater architecture," *Physical Review A*, vol. 92, no. 2, 022 357–undefined, Aug. 2015, ISSN: 10941622. DOI: 10.1103/PhysRevA.92.022357. [Online]. Available: https://journals.aps.org/pra/abstract/10.1103/PhysRevA.92.022357.

[14] N. Sinclair, E. Saglamyurek, H. Mallahzadeh, J. A. Slater, M. George, R. Ricken, M. P. Hedges, D. Oblak, C. Simon, W. Sohler, and W. Tittel, "Spectral multiplexing for scalable quantum photonics using an atomic frequency comb quantum memory and feed-forward control," *Physical Review Letters*, vol. 113, no. 5, pp. 053 603–1, Jul. 2014. DOI: 10.1103/PhysRevLett.113.053603. arXiv: 1309.3202. [Online]. Available: http://dx.doi.org/10.1103/PhysRevLett.113.053603.

[15] G. Avis, In preparation, 2021.

[16] T. Coopmans, R. Knegjens, A. Dahlberg, D. Maier, L. Nijsten, J. Oliveira, M. Papendrecht, J. Rabbie, F. Rozpędek, M. Skrzypczyk, L. Wubben, W. de Jong, D. Podareanu, A. T. Knoop, D. Elkouss, and S. Wehner, "NetSquid, a discrete-event simulation platform for quantum networks," Oct. 2020. arXiv: 2010.12535. [Online]. Available: http://arxiv.org/abs/2010.12535.

[17] C. M. Caves, C. Zhu, G. J. Milburn, and W. Schleich, "Photon statistics of two-mode squeezed states and interference in four-dimensional phase space," *Physical Review A*, vol. 43, no. 7, pp. 3854–3861, Apr. 1, 1991. DOI: 10.1103/PhysRevA.43.3854. [Online]. Available: https://link.aps.org/doi/10.1103/PhysRevA.43.3854 (visited on 05/05/2021).

[18] D. Maier, *Snippet for various atomic ensembles (AE) components used in a quantum network*, Apr. 2021. [Online]. Available: https://gitlab.com/softwarequtech/netsquid-snippets/netsquid-ae.

A Parameters

Name	Value	Description
num_repeaters	0	Number of repeaters in the chain.
multi_photon	true	Whether to include multi-photon emission in the simulation.
num_attempts	-1	Number of clicks after which the clock stops.
num_attempts_proto	-1	Number of clicks after which the emission protocol stops.
num_successes	1e5	Number of successes after which the simulation is stopped.
collect_states	false	Whether to collect end-to-end states.
encoding	presence_absence	Type of encoding used.
clock	1e5	Time between ticks of the clock (in ns).
magic	forced	Whether to use magic to create elementary link states.
multiple_link_successes	false	Whether to allow for multiple successful modes.
Sources		
mean_photon_number	*varied*	Mean photon number of the source.
emission_probabilities	None	Probability distribution of multi-photon emissions.
source_frequency	1e5	Frequency of the photon source.
Memories		
memory_time_dependence	exponential	Time dependence of memory.
spectral_modes	1	Number of spectral modes the source can produce.
temporal_modes	1	Number of temporal modes the source can produce.
spatial_modes	1	Number of spatial modes the source can produce.
max_memory_efficiency	1.0	Maximum efficiency of the memory if a photon would be retrieved immediately.
memory_coherence_time	.inf	Coherence time of the memory.
Channels		
length	*varied*	Total length of the elementary link.
asymmetry	*varied*	Value of midpoint asymmetry.
channel_length_l	*varied*	Length of the left channel (km).
channel_length_r	*varied*	Length of the right channel (km).
attenuation_l	0.2	Fiber attenuation of the left channel (dB/km).
attenuation_r	0.2	Fiber attenuation of the right channel (dB/km).
coupling_loss_l	0.0	Initial loss probability of the left channel.
coupling_loss_r	0.0	Initial loss probability of the right channel.
fibre_phase_stdv_l	0	Standard deviation of the gaussian distribution of the phase for `PhaseLossModel` on the left channel.
fibre_phase_stdv_r	0	Standard deviation of the gaussian distribution of the phase for `PhaseLossModel` on the right channel.
Midpoint Detectors		
mid_det_efficiency	1.0	Detection efficiency.
mid_det_visibility	1.0	Photon indistinguishability at the midpoint BSM.
mid_det_num_resolving	false	Whether are midpoint detectors number-resolving.
mid_det_dark_count_prob	0.0	Dark count probability at each midpoint detector.
Swap Detectors		
swap_det_num_resolving	false	Whether are swap detectors number-resolving.
swap_det_dark_count_prob	0.0	Dark count probability at each swap detector.
swap_det_efficiency	1.0	Detection efficiency.

Table 1: Table with all simulation parameters. Value of *varied* means the parameter is varied when looking for the optimal mean photon number.

B Plots with Symmetric Mean Photon Pair Numbers

Plots for elementary link with total length of 50 km can be found in Figure B.1 and B.2. For the elementary link of 25 km, we only show the plots for SKR in Figure B.3.

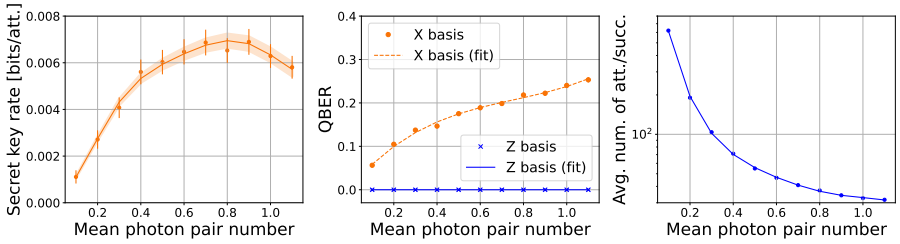

(a) $A = 0.1$

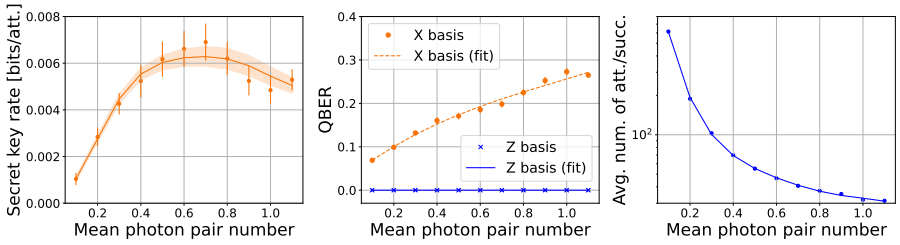

(b) $A = 0.2$

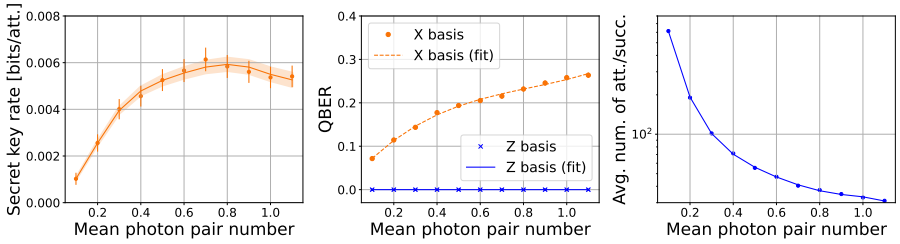

(c) $A = 0.3$

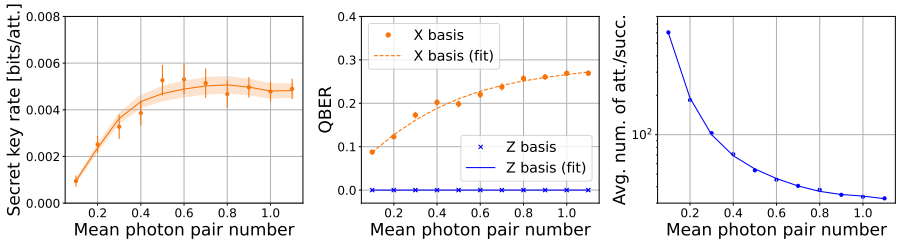

(d) $A = 0.4$

Figure B.1: Results for elementary links of 50 km with presence-absence encoding for varying degrees of asymmetry A. Sources have the same mean photon pair number. Simulation is run until there are 10000 successful entanglement generation attempts. Cases of $A = 0$ and $A = 0.5$ are shown in Figure 4.1.

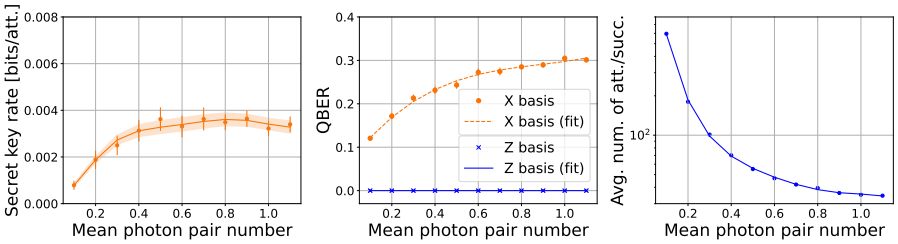

(a) $A = 0.6$

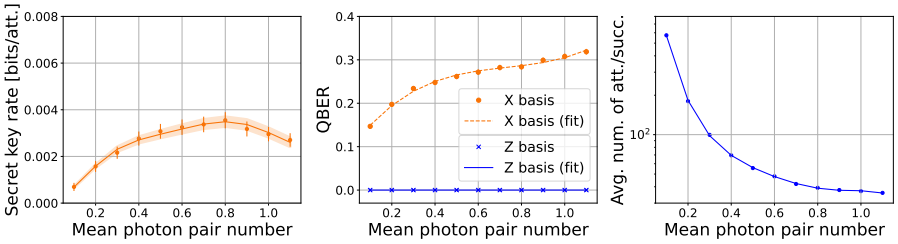

(b) $A = 0.7$

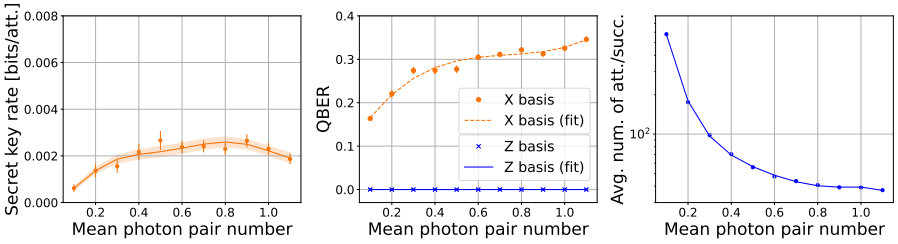

(c) $A = 0.8$

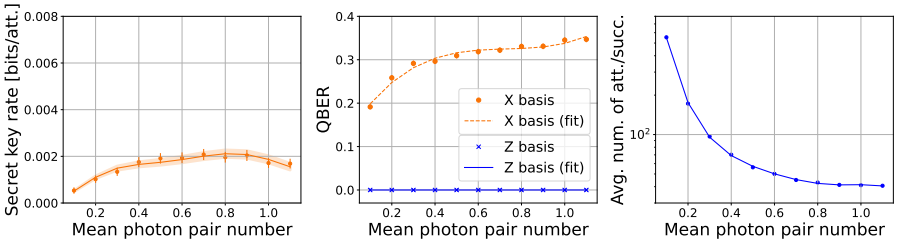

(d) $A = 0.9$

Figure B.2: Results for elementary links of 50 km with presence-absence encoding for varying degrees of asymmetry A. Sources have the same mean photon pair number. Simulation is run until there are 10000 successful entanglement generation attempts. The scales are same in all sets of plots.

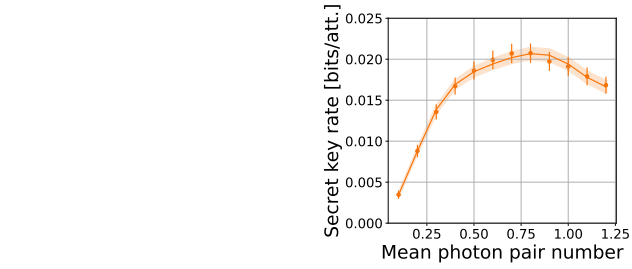

(a) $A = 0$

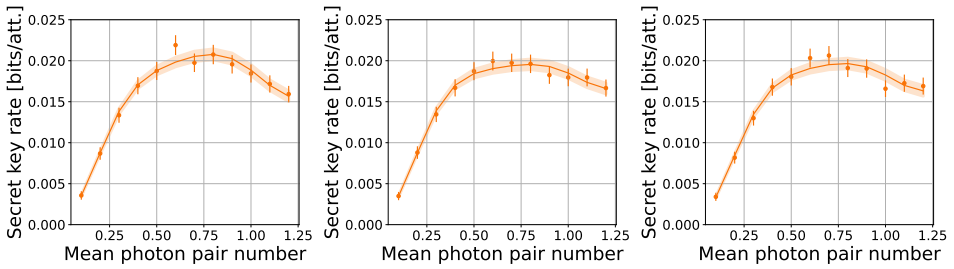

(b) $A = 0.1$ (c) $A = 0.2$ (d) $A = 0.3$

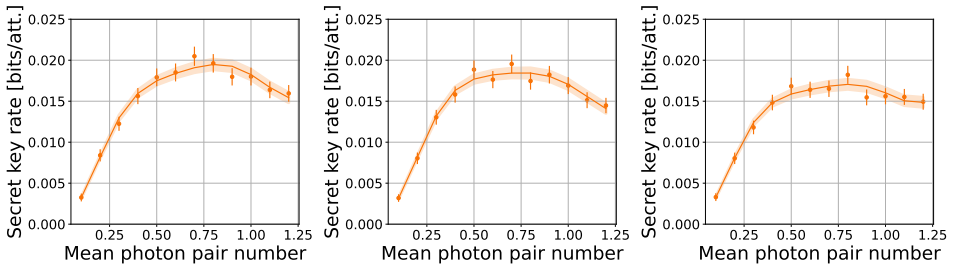

(e) $A = 0.4$ (f) $A = 0.5$ (g) $A = 0.6$

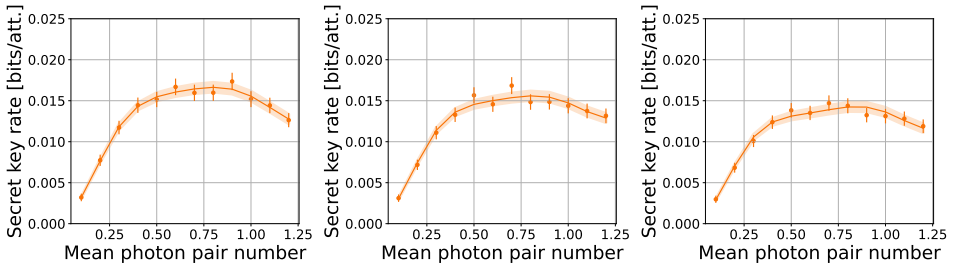

(h) $A = 0.7$ (i) $A = 0.8$ (j) $A = 0.9$

Figure B.3: Results for elementary links of 25 km with presence-absence encoding for varying degrees of asymmetry A. Sources have the same mean photon pair number. Simulation is run until there are 10000 successful entanglement generation attempts. The scales are same in all sets of plots.

C Plots with Asymmetric Mean Photon Pair Numbers

Figure C.1 shows plots of SKR for elementary link with total length of 50 km for the case where we allow the two sources to have asymmetric mean photon pair numbers.

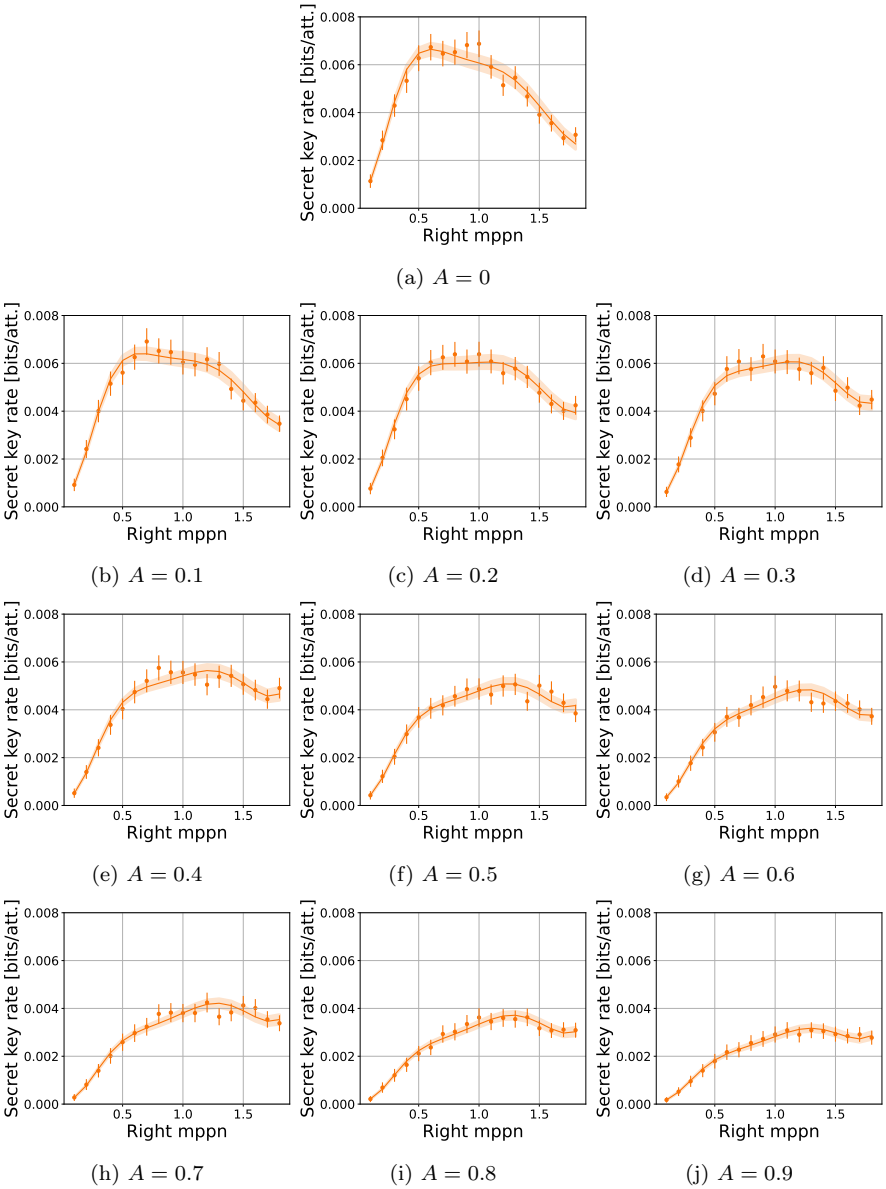

(a) $A = 0$

(b) $A = 0.1$ (c) $A = 0.2$ (d) $A = 0.3$

(e) $A = 0.4$ (f) $A = 0.5$ (g) $A = 0.6$

(h) $A = 0.7$ (i) $A = 0.8$ (j) $A = 0.9$

Figure C.1: Results for elementary links of 50 km with asymmetric mean photon pair numbers and presence-absence encoding for varying degrees of asymmetry A. The x-axis shows the value of the right mppn while the left mppn can be calculated from the heuristic introduced in Section 4. Simulation is run until there are 10000 successful entanglement generation attempts.